PERGAMON

International Journal of Solids and Structures 40 (2003) 6023–6042

INTERNATIONAL JOURNAL OF SOLIDS and STRUCTURES

www.elsevier.com/locate/ijsolstr

Interfacial mixed-mode fracture of adhesive bonds undergoing large deformation

Herzl Chai *

Department of Solid Mechanics, Materials and Systems, Faculty of Engineering, Tel Aviv University, Tel Aviv 69978, Israel

Received 20 December 2002; received in revised form 1 July 2003

Abstract

Interfacial fracture of adhesive bonds undergoing large-scale yielding is studied using a combined experimental/finite-element approach. The full range of in-plane mode mixity is produced over bond thickness ranging from 30 to 500 μm using the scarf and the ENF joint geometries. Novel techniques for introducing pre-cracks and surface decoration, together with in situ observations, facilitate accurate determination of the bond-average and the local shear strains at the crack tip during the onset as well as the rest of the crack propagation event. The crack generally grew along one of the two interfaces of the bond, although the failure was always fully cohesive. The local shear strain at the crack tip is *independent* of the bond thickness, and, under quasi-static conditions, it remains constant *throughout* the growth, which make it a viable fracture parameter. This quantity strongly depends on the mode mixity, the sign of the phase angle (i.e., shearing direction) and the crack speed, however.

A finite-element analysis is used to obtain the crack tip deformation field for an interface crack in adhesively bonded scarf and ENF joints. Large-strain and quasi-static conditions are assumed. A distinct material model in the fracture process zone that allows for volume change in the post-yield regime is incorporated into the analysis. The local deformation is characterized by a pair of bond-normal and tangential displacements corresponding to the nodal points adjacent to the crack tip. The critical values of these quantities are obtained when the FEM *bond-average* shear strain at the crack tip becomes equal to its experimental counterpart. The so defined critical local displacements, after an appropriate normalization, seem to conform to a single-valued, linear type interrelationship over the entire range of mode mixity. The fact that this relationship is independent of the bond thickness, and furthermore it encompasses both cases of positive and negative phase angles, makes it a viable candidate for characterizing mixed-mode interfacial fracture under large-deformation conditions.

Keywords: Adhesive bonds; Fracture; Mixed-mode; Interface; Plasticity; Cohesive zone

1. Introduction

The fracture resistance of adhesive bonds is a subject of interest in a variety of technological and industrial applications, including traditional adhesive bonding, laminated composites and electronic circuit

* Tel.: +972-36408342; fax: +972-36407617.
E-mail address: herzl@eng.tau.ac.il (H. Chai).

0020-7683/$ - see front matter © 2003 Elsevier Ltd. All rights reserved.
doi:10.1016/S0020-7683(03)00398-6

boards. Such fracture is complex and interactive, depending on the mode mixity, the strength of the interface, the thickness and ductility of the interlayer, and other parameters. These difficulties notwithstanding, the adhesive bond configuration entails a number of simplifications that makes it a viable and efficient mean for exploring fracture phenomena in general. First, the plastic deformation is confined to the interlayer region. Second, by systematically varying the bond thickness, a number of technologically important fracture problems can be addressed (Chai, 1988, 1992, 1993a). When the bond thickness is large compared to the plastic deformation zone at the crack tip, as occurs for a weak interface or a highly brittle adhesive, the case of bi-material interface crack is realized. In the other extreme end of very thin bonds, the natural deformation at the crack tip is drastically suppressed. This leads to an extended plastic deformation zone that may be several orders of magnitude greater than the bond thickness. This phenomenon, which typifies even highly brittle adhesives, the more so with increasing the shear component of the loading, directly bears on interlaminar fracture of laminated composites (Chai, 1990). Between these two extremes, a partial interaction of the intense deformation zone at the crack tip and the confining surfaces of the adherends occur. It is for this extended volume of plastic deformation or energy dissipation that traditional adhesive bonds are designed in this intermediate thickness range (e.g., 50–150 μm).

The majority of fracture analyses of adhesive bonds are based on the concept of fracture energy. The latter combines fundamental material properties such as strength (yield) and deformation (ultimate strain) into a valuable engineering design parameter without a need to resort to the local deformation details at the crack tip. Experiments show, however, that the fracture energy is strongly dependent on the bond thickness, and furthermore it exhibits a geometry-dependent resistance behavior prior to attaining steady-state growth (Brandenburger and Pearson, 1995; Pang and Seetoh, 1997; Chai, 1988; Ikeda et al., 2000; Madhusudhana and Narasimhan, 2002). To possibly circumvent these difficulties, the local energy absorption in the fracture zone needs to be isolated from the geometry-dependant, global or structural energy dissipation mechanisms. Important advances toward this goal were made in recent studies of bi-material interface crack problems, which are a special case of the present configuration. Needleman (1987) proposed a cohesive zone model in which the plane of the crack is held by a spring-like entity possessing a built in traction-separation law. Extension of this model to fracture under mixed-mode conditions was given by Tvergaard and Hutchinson (1993). According to this idea, fracture occurs when the normal and the tangential displacements at the tip of the cohesive zone fulfill a certain interactive criterion. More recently, Tvergaard and Hutchinson (1994) extended the cohesive zone model to mixed-mode fracture of adhesive bonds. Yang and Thouless (2001) proposed a modified approach in which the opening and shearing displacements in the cohesive zone are such that the intrinsic toughness of the interface is mode-dependent. At its present development stage, the cohesive zone concept seem to be limited somewhat by the lack of a sound experimental procedure for quantifying some of its parameters, and by the fact that the traction-separation law must be a priori prescribed. The latter constraint may be especially disadvantageous when large-scale yielding and strain-hardening response are involved, as is the case here.

For a viable geometry independent fracture criterion in the large-deformation regime, quantitative information on the local fracture process would be helpful. Because of the smallness of the deformations involved, it is often necessary to complement measurements with numerical or analytical analyses. Liechti and Knauss (1982) were among the first researchers to adopt such a combined approach in their study of a rubber adhesive subject to mixed-mode loading. In this work, the opening displacement behind the crack tip was measured with the aid of an interferometer while the shearing counterpart derived analytically. More recently, a technique for measuring local shear strains, based on the deformation of fine lines that are scratched onto the observed surface of the specimen, was developed and applied to structural adhesive joints subject to pure mode II loading (Chai, 1993a; Chai and Chiang, 1996). The result show that the critical shear strain at the crack tip is independent of the bond thickness and, excluding rate effects, is fixed throughout the crack propagation event. It is the purpose of this work to extend such approach to general mixed-mode conditions.

A full-fledged mixed-mode study of adhesive bonds entailing all the three components of fracture appears prohibitive. Fortunately, the problem can be greatly simplified by taking advantage of the coincidence of the mode II and mode III fracture energies in this case (Chai, 1988); although on the microscale level these quantities may entail different microcrack patterns, both are dominated by plastic shearing. Thus, a mode I–mode II study may suffice. In this work, the end-notched flexure (ENF) specimen and the scarf joint are used in order to produce the full range of in-plane mode mixity. The adhesive is a toughened epoxy, with its thickness being a prime experimental variable. A new technique for introducing a sharp interfacial pre-crack in the bond facilitates quantitative measurements of the local shear strain at the onset as well as the rest of the fracture event. The latter is recorded in real-time using a long-range optical microscope. The results of these careful measurements serve as the basis for developing a physically sound local fracture approach.

The experiments are reported in Section 2. A large-strain finite-element analysis (FEA) is employed to obtain the deformation field at the crack tip (Section 3). The analysis employs a cohesive-zone-like model allowing for volumetric change in the highly strained region in the cracked bond. Critical local displacements for crack propagation are generated from the FEA based on the critical bond-average shear strain that is obtained from the tests. While the emphasis in this work is placed on the local deformation at the crack tip, some discussions of the results in the context of fracture energy is given in Section 4.

2. Experimental

2.1. Materials and apparatus

The majority of mixed-mode adhesive bond specimens reported in the literature are constructed of beam type elements (Chai, 1992; Ferlund and Spelt, 1994; Brandenburger and Pearson, 1995; Ducept et al., 2000). In addition to their inherent ability to produce stable crack growth, such designs may also allow for the determination of the individual fracture energy components with the aid of easily measured global quantities such as load and deflection. These advantages are somewhat muted, however, when large deformations in the adhesive are involved. Another viable test specimen used to study mixed-mode fracture of adhesive bond is the compact tension shear specimen (Chowdhury and Narasimhan, 2000; Deepankar and Narasimhan, 1998), which, in effect, may be regarded as a modified Arcan type specimen. In this work, the scarf joint shown in Fig. 1a, first introduced by Trantina (1972), and latter employed by Bascom and Oroshnik (1978), is used. By varying the scarf angle, θ, the full range of mode mixity can be generated. This geometry generally leads to an unstable crack growth, but for the present ductile adhesive, a phase of slow growth always preceded rapid propagation. Such growth is useful in that it allows for continues measurements over time to be made. To maintain a form of symmetry, a central crack is adopted instead of the single edge crack used by Trantina. The limit case of pure mode II is obtained using the ENF specimen, first introduced by Barret and Foschi (1977) for studying mode II fracture of wood, and latter extended to laminated composites (Russell and Street, 1987) or adhesive joints (Chai, 1988). As shown in Fig. 1b, the present specimen consists of two flat, 20 mm wide aluminum bars that bond the adhesive of interest. To prevent plastic deformation outside the bond area, the adherends are reinforced with hardened steel bars via a set of screws. A number of aluminum alloys were considered for the adherends, including 7075, 2024, 5052 and 5086. The latter, which contains the least amount of additives, has resulted in a fully cohesive failure, and is thus adopted for this study. The bonding surfaces are first polished and then chemically etched in accordance with the FPL (Forest Products Laboratory) procedure. This generates a porous oxide layer on the bonding surfaces, which enhances bonding through mechanical interlocking. The adhesive is Cycom BP-907 (American Cyanamid), a mildly ductile, modified epoxy resin.

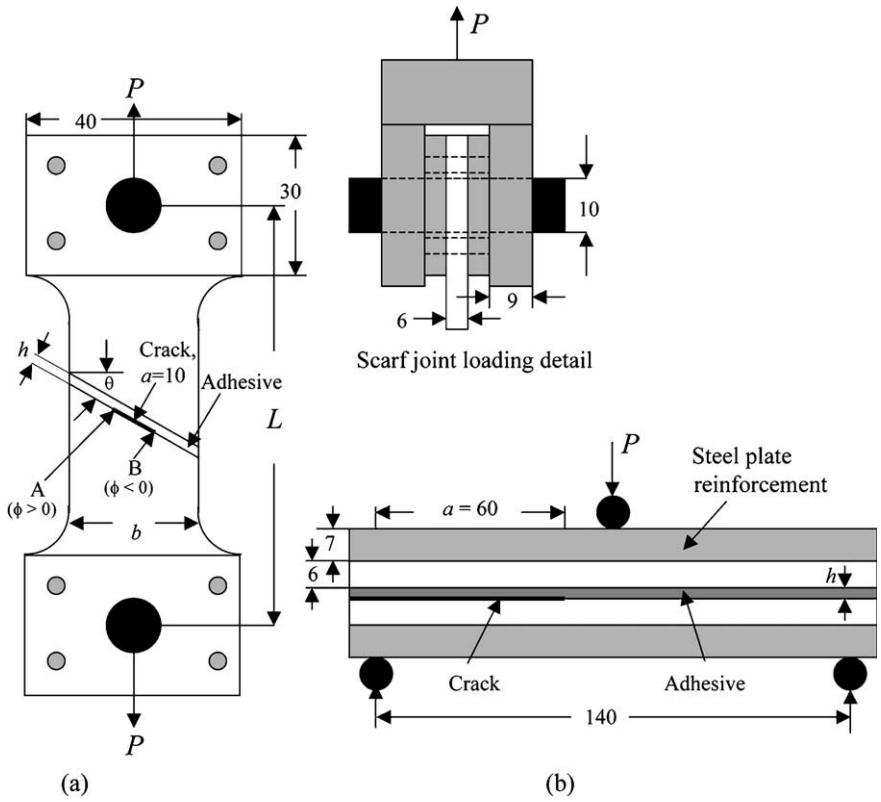

Fig. 1. Schematics of the scarf (a) and ENF (b) adhesive joint test specimens. The crack tips denoted by points A and B correspond to the shearing of the adhesive in the crack propagation direction and opposite to it, respectively, or positive and negative phase angles, respectively. All dimensions are in mm.

Introducing a sharp pre-crack is essential for obtaining meaningful local deformation data at the *onset* of crack propagation. Initial cracks are generally formed using Kapton or Teflon film separators. This typically results in a relatively thick crack (>10 μm) which location within the bond is not easily controlled. A comprehensive study was carried out in an effort to produce a thin, discriminatory weak interface. Techniques such as sputter coating, Teflon spraying and foil wrapping were used and found not fully satisfactory. The method finally adopted was to scrub the adherend surface over the initial crack area with a soft lead pencil. This results in a sharp interfacial crack that typically popped out at less than 50% of the critical load for crack extension. We differentiate between the crack tips marked A and B in Fig. 1a, for which the adhesive is sheared along the crack propagation direction and opposite to it, respectively; in the context of LEFM, these conditions are often associated with $\phi > 0$ and $\phi < 0$, respectively, where ϕ denotes the phase angle. The present tests show that the fracture behavior is greatly influenced by the shearing direction or the sign of ϕ, the effect that increases with the intensity of the deformation.

Scarf joints are fabricated using various scarf angles in the range 20–80° and bond thickness in the range 30–500 μm. Fig. 1a and Table 1 lists the scarf joint configurations used; for all cases, the out-of-plane dimension of the adherends is 5 mm. The bond thickness, h, is controlled by spacers that are placed outside the final bond region. Special care is taken to insure uniformity of the bond. Following curing in an oven at 177 °C, the specimens are machined off to their final dimensions as listed in Table 1. The observed side of the bond is polished to 1 μm surface quality. The bond thickness is measured from both sides of the bond using an optical microscope; thickness variations exceeding 10% are rejected for data analysis. The viewing

Table 1
Scarf joint geometry and associated experimental data*

L (mm)	b (mm)	θ°	$(\gamma_{Av}, \phi^\circ)$ $h = 50$ μm, $\phi > 0$	$(\gamma_{Av}, \phi^\circ)$ $h = 50$ μm, $\phi < 0$	$(\gamma_{Av}, \phi^\circ)$ $h = 200$ μm, $\phi > 0$	$(\gamma_{Av}, \phi^\circ)$ $h = 200$ μm, $\phi < 0$	(γ, ϕ°) $\phi > 0$	(γ, ϕ°) $\phi < 0$
138	40	30	(0.11, 50.9)	(0.11, −50.3)	(0.05, 50.8)	(0.05, −51.3)	(0.3, 51.1)	(0.16, −51.3)
130	34	45	(0.205, 68.1)	(0.205, −68.2)	(0.08, 65.8)	(0.08, −67.7)	(0.5, 66.8)	(0.28, −68)
136	34	60	(0.3, 76.5)	(0.3, −80.1)	(0.1, 74.3)	(0.1, −77)	(0.82, 66.8)	(0.4, −78.4)
166	20	70	(0.31, 80.7)	(0.31, −84.6)	(0.11, 79.7)	(0.11, −82.3)	(1.0, 80.6)	(0.47, −83.1)
200	20	80	(0.31, 89.2)	(0.31)	(0.11)	(0.11)	(1.19, 85)	(0.6, −89.4)
N/A	N/A	90	(0.31, 90)	(0.31, −90)	(0.11, 90)	(0.11, −90)	(1.33, 90)	(0.7, −90)

*γ and γ_{Av} are, respectively, the experimentally-obtained critical local and bond-average shear strains at the crack tip; ϕ is the loading phase angle ($= a\tan(\gamma_{AV}/\varepsilon_{Av})$); the case $\theta = 90^\circ$ correspond to the ENF geometry (Fig. 1b).

edge of the bond is then painted with a diluted white correction fluid to give a micron thick diffusive coating. A series of fine lines are then scratched on the observed edge of the specimen, normal to the bondline, using a specially designed apparatus composed of a traveling scalpel that is attached to a ball bearing. In this way, lines as thin as 2 μm could be produced. The line spacing was typically a fraction of the bond thickness. The ENF specimens are similarly fabricated according to the details shown in Fig. 1b.

The scarf joints are pin-loaded at both ends while the ENF specimens are loaded in a three-point bending scheme. The loading commences at a slow crosshead rate (0.1 mm/s) using an Instron tensile tester. A zoom optical microscope (Questar, Inc.) in conjunction with a video camera is used to observe in real-time the crack tip region. With this system, screen magnifications of up to 500 could be achieved. The microscope is mounted on an X–Y–Z platform that in turn is situated atop a stage which angle of inclination can be set to any desired angle. The fracture behavior for the positive and the negative phase angles are established by observing during the test either the crack tip marked A or B in Fig. 1. The load is recorded during the tests using a side camera whose image is incorporated into the main frame. Over hundred scarf joints and ENF specimens are tested.

2.2. Test results

Figs. 2 and 3 shows two sequences of micrographs exemplifying the fracture process for the case in which the adhesive is sheared in the crack propagation direction ($\phi > 0$) and opposite to it ($\phi < 0$), respectively; the joint parameters and the loading direction are noted in each figure. Note that the right hand side prints in Fig. 2 are magnifications of the prints to the left. The first frame in each sequence corresponds to the onset of crack propagation, and is assigned the time $t = 0$. As shown in Fig. 2, the crack propagates along the interface up to catastrophic growth, which occurs just prior to frame III. In the early stages of crack propagation, the plastic deformation zone, manifested by the large distortion of the initially bond-normal scratch lines, is highly concentrated. As the crack continues to grow, this deformation spreads out. The fracture behavior for $\phi < 0$ (Fig. 3) is generally similar except that the crack kicks out toward the opposing interface once growth occurs. One also observes from both micrograph sequences that the material at the immediate crack tip vicinity display some forms of damage and voids. Such observations motivate our forthcoming use of a distinct material model at the crack tip region.

The distortion of the initially bond-normal scratch lines during the loading affords a viable measure of local deformation quantities. We define "average" and "local" shear strains in the adhesive as the relative

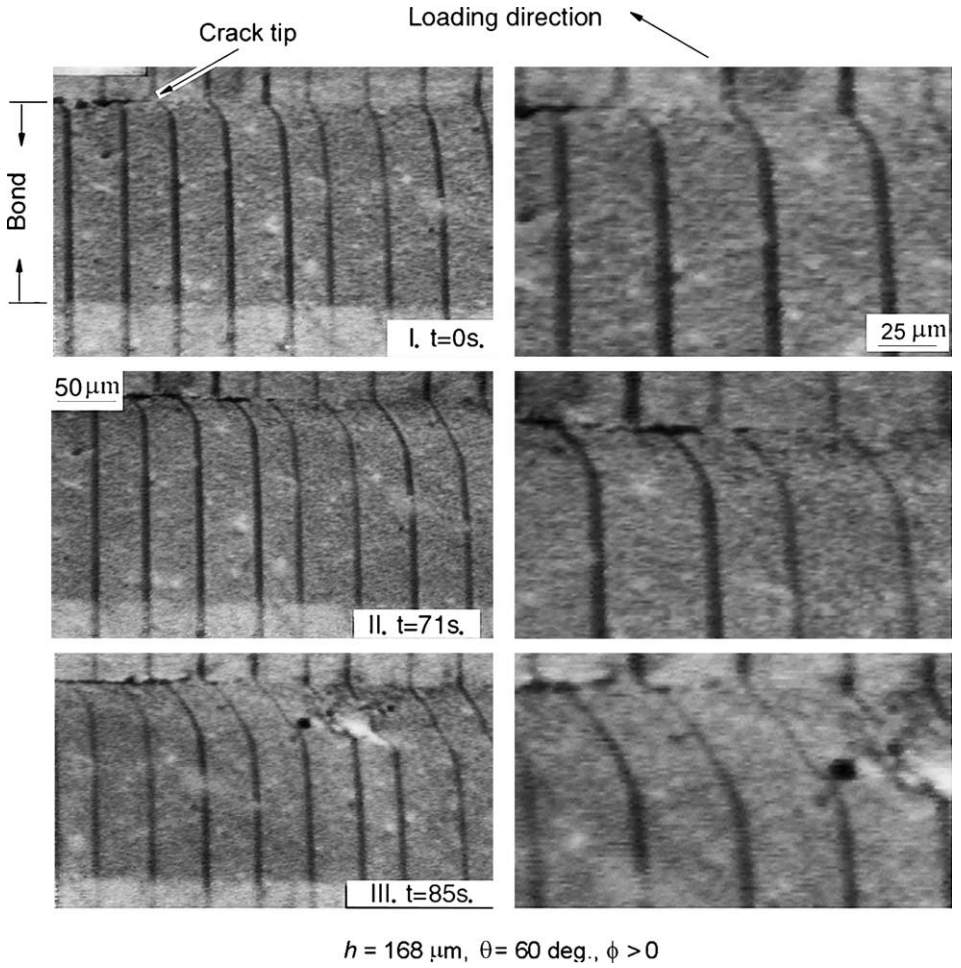

Fig. 2. A micrograph sequence of the crack tip region for a positive phase angle, $h = 168$ μm, $\theta = 60°$; the prints on the right are enlargements of the prints on the left. The first and last frames in each sequence correspond to the onsets of crack propagation and rapid growth, respectively. The series of scratch lines in the prints are initially normal to the bondline.

shear displacement across the bond divided by the bond thickness and the slope of the scratch line, respectively. Naturally, we will focus on the value of these quantities at the crack tip region. While the average shear strain, denoted as γ_{Av}, can be easily measured from the distortion of the scratch lines, the determination of the local shear strain at the crack tip, γ, is less straightforward if one assumes that the measured value is dependent on the scale of the observation. Enlargements of the crack tip regions (e.g., right hand side of Fig. 2) reveal, however, that the scratch lines tend to form a finite, constant slope as they approach the crack tip. This property allows for meaningful measurements of local engineering shear strain to be made. [1] To increase

[1] In a previous study (Chai, 1993b), the ultimate shear strain of the present adhesive was measured as a function of bond thickness using the Napkin Ring test specimen The results show that as the bond thickness is decreased to a few micrometers, the ultimate shear strain tends to reach a plateau. The fact that the magnitude of this plateau, which was interpreted as an intrinsic material property, is similar to the critical local shear strain, γ, obtained in the present mode II tests (results to be reported in Fig. 5), is supportive of the above constant slope assertion.

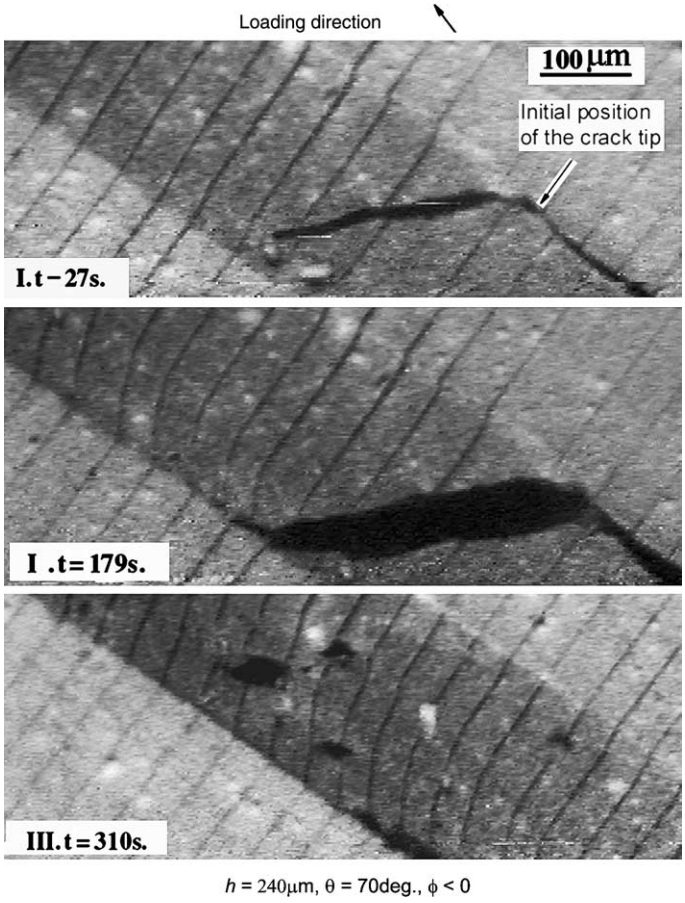

Fig. 3. A micrograph sequence of the crack tip region for initially negative phase angle, $h = 240$ μm, $\theta = 70°$. The first and last frames in each sequence correspond to the onsets of crack propagation and rapid growth, respectively.

accuracy, the shear strains so defined are determined with the aid of a robust digital image-processing package.

During a typical test, the deformation in the bond is built up until a critical load for crack propagation is reached. From micrographs such as shown in Figs. 2 and 3, the variation with time of the crack extension, Δ_a, and the local (γ) and bond-average (γ_{Av}) shear strains at the crack tip can be determined. Fig. 4 shows typical results for two scarf joints pertaining to $\phi > 0$ and $\phi < 0$ In both the cases, the data start with the onset of crack propagation and end with the onset of rapid or catastrophic growth. The crack tends to accelerate following an initial phase of slow growth, with γ_{Av} steadily increasing, virtually matching, in the case of Fig. 4a, the local shear strain, γ, at the onset of rapid crack propagation. [2] On the other hand, the local shear strain varies only little during the growth. In fact, a detailed study of all the crack histories in this work showed that the source of the latter variations is due mostly to rate effects. The dependence of the

[2] A detailed examination of the test results show that the attainment of a state of uniform shear strain across the bond at onset of rapid crack propagation is limited to relatively thin bonds (i.e., less than about 100 μm) and relatively large scarf angles (i.e., >45°). Beyond this range, catastrophic growth generally occurred prior to the coincidence of γ_{Av} and γ.

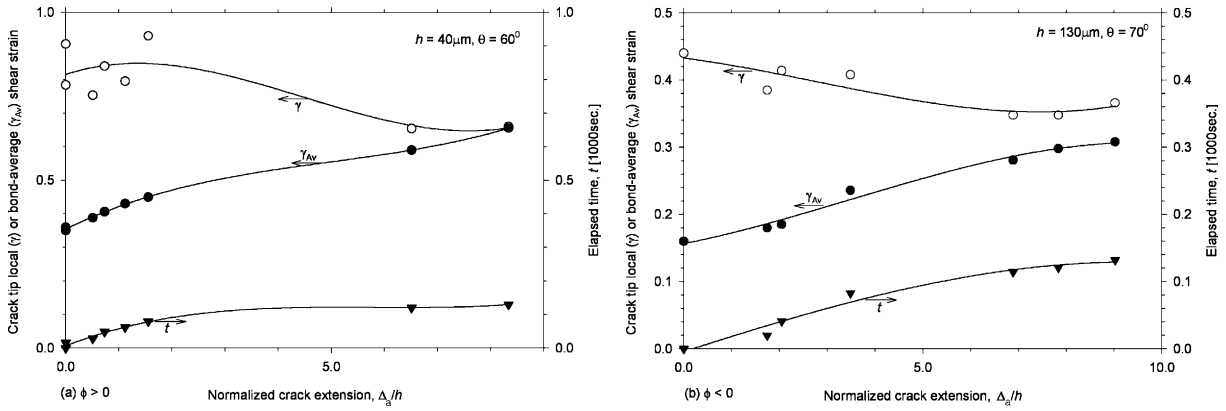

Fig. 4. The variations of elapsed time, local, and average shear strains at the crack tip with normalized crack extension for two representative tests: (a) positive phase angle, $h = 40$ μm, $\theta = 60°$, (b) negative phase angle, $h = 130$ μm, $\theta = 70°$. The first and last data point in each figure corresponds to the onsets of crack propagation and steady-state or rapid growth, respectively. The solid lines are possible fits to the data.

instantaneous local shear strain, γ, on the crack speed, v, was determined by considering isolated segments in the crack growth history, where the crack speed was fairly constant. Combined results from all the tests performed show that for a given scarf angle, the local shear strain monotonically decrease with increasing the crack speed, reaching a plateau which is approximately 65% of the quasi-static value (i.e., at $v \to 0$) once v is increased from approximately 10 μm/s. It was found that the combined data are reasonably well fitted by the following relation:

$$\gamma(\theta, v)/\gamma(\theta, v = 0) = 1 - \alpha(1 - e^{-\beta v}), \quad \alpha = 0.35, \quad \beta = 0.2 \text{ s}/\mu\text{m} \tag{1}$$

where $\gamma(\theta, v)$ is the critical local shear strain pertaining to a scarf angle θ for a crack propagating at a speed v. It should be noted that this relation is quite similar to that obtained for the pure mode II case (Chai and Chiang, 1996).

Fig. 5 shows the dependence of the critical local shear strain on the bond thickness and the scarf angle for all the tests performed. The data corresponds to the *onset* of crack propagation, where rate effects are negligible. (The crack typically started to grow a few minutes after the application of the load). However, as discussed in Fig. 4 and Eq. (1), these data should be also applicable to the entire crack growth history under conditions of quasi-static growth. Experimental scatter due to inaccuracy in measuring the slope of the scratch lines are deemed less than 10%. A good indication of this scatter is in fact afforded by the wealth of data presented. As shown, the data for the scarf joints cover nearly the entire range of mode mixity, with those for $\theta = 80°$ not far from the ENF results, identified by $\theta = 90°$ in the figure. It should be noted that the data for the scarf joints are limited to $\theta > 20°$ because of difficulties in resolving the small slopes involved for shallower scarf angles. For a given θ, γ seems independent of the bond thickness, being about twice as large for the positive phase angle (Fig. 5a) as compared to the negative phase angle (Fig. 5b). To manifest these effects visually, the data for each scarf angle are fitted by a straight, dotted line. The results show that γ increases with the scarf angle, being as large as 1.3 in the case of pure mode II loading pertaining to $\phi > 0$.

It is of interest to express the mixed-mode conditions in terms of crack tip parameters rather then the scarf angle. The bond-average tensile and shear strains at the crack tip are natural choices for this purpose. Define a local "loading" phase angle, ϕ, as

$$\tan\phi = \gamma_{\text{Av}}/\varepsilon_{\text{Av}} \tag{2}$$

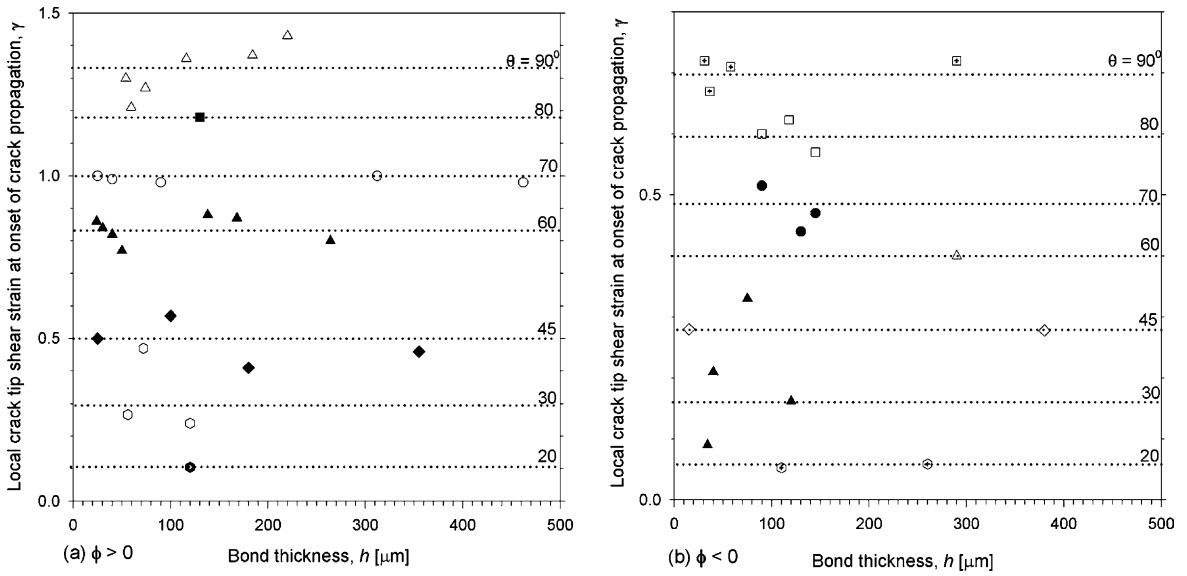

Fig. 5. Experimental *local* crack tip shear strain at onset of crack propagation as a function of bond thickness, for various scarf angles: (a) positive phase angle, (b) negative phase angle. Dotted lines are possible fits to the data.

It can be easily shown from geometrical consideration that $\phi = \theta$ in the case of homogeneous scarf joint (e.g., Suo and Hutchinson, 1989). [3] For the present configuration, because of the deformation and rotation that are incurred by the adherends during the loading, this relation is not fully maintained (Section 3.2). The bond-average shear strain at the crack tip, being relatively large, could be easily determined from the tests (e.g., Fig. 4). Table 1 summarizes the results at *onset* of crack propagation for two representative bond thickness, i.e., 50 μm and 200 μm. Because the bond-average tensile strain is too small to be measured accurately in our tests, the FEA (Section 3.2) is employed to infer this quantity. Using Eq. (2), the value of the loading phase angle at onset of crack propagation can then be determined, and the results given in Table 1. Fig. 6 (filled symbols) plots the variation of γ_{Av} with ϕ from Table 1 for the two bond thickness under discussion, where symbols and broken line curves denote individual data points and their possible fits, respectively. The critical bond-average shear strain for a given bond thickness exhibit a sigmoidal type variations with the phase angle, being quite symmetric with respect to the sign of ϕ. As shown, reducing the bond thickness increases the value of γ_{Av} needed to cause crack propagation. This effect implies that the bond-average strain at the crack tip is inadequate as a universal fracture criterion. Nevertheless, as will be seen latter in this work, these data provide the basis for predicting the critical *local* displacements in the FEA.

With the aid of Fig. 5 and Table 1, the experimental *local* shear strain at the crack tip can be presented as a function of the "loading" mode mixity parameter ϕ rather than the scarf angle θ. The results are shown numerically in Table 1 and figuratively in Fig. 6 (open squares). The critical local shear strain, which may be viewed as the thin-bond limit case of the bond-average results, exhibits a large asymmetry with respect to the sign of the phase angles. As shown by the associated solid line curve, a reasonable fit to the local shear strain is given by

[3] Note that under small-scale yielding (and a homogeneous type scarf joint), the right hand side of Eq. (2) equals K_{II}/K_I the ratio of mode II and mode I stress intensity factors. The phase angle can be corrected for material discontinuity across the interface, but the benefit of this in the context of large deformation is questionable.

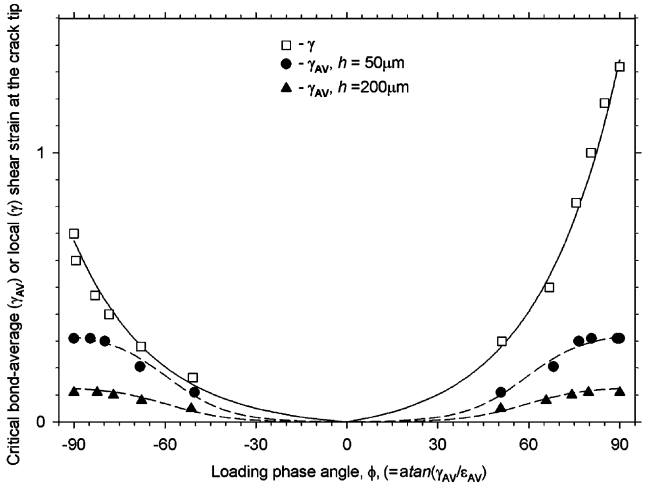

Fig. 6. Experimental local (open symbols) and bond-average (filled symbols) shear strains at the crack tip at onset of crack propagation as a function of the experimentally obtained loading phase angle. The results for γ_{Av} are given for 50 and 200 μm thick bonds. Curves are possible fits to the data.

$$\gamma = A(e^{B\phi} - 1), \quad \phi > 0 \tag{3a}$$

$$\gamma = 0.5A(e^{-B\phi} - 1), \quad \phi < 0 \tag{3b}$$

where A and B are constants, given as 0.05 and 2.12/rad., respectively. These results will be discussed further in Section 4, in connection with the fracture energy of the joint.

3. Finite-element analysis

3.1. Problem definition

A commercial finite-element code (Ansys, Version 5.7) is used to model the specimens shown in Fig. 1. In the case of the scarf joint, a 10 mm long crack is placed at the center of the lower interface of the bond. The tips of the crack at points A and B are associated with positive and negative phase angles, respectively; such distinction is necessary in light of the departure of the results of Fig. 5a and b. The full scarf joint geometry is used in the FEM model in order to account for the rotation and deformation incurred by the adherends. The dimensions of the specimen analyzed are the same as used in the tests (Table 1). The case of pure mode II loading is generating from the scarf joint geometry by stipulating a 0° scarf angle and rigid adherends, and by applying a shearing displacement across the bond instead of the vertical pull. The adherends are assumed linearly elastic, with Young's modulus, E_s and Poisson's ratio, v_s, equal 70 GPa and 0.25, respectively. The elastic constants for the adhesive are $E_a = 3.15$ GPa and $v_a = 0.35$. Modeling the post-yield behavior of the adhesive is a bit involved. The stress–strain relation in simple shear for this material was determined as a function of the bond thickness, i.e., from 5 μm to 500 μm, using the Napkin Ring test (Chai, 1993b). The adhesive response was found to be sensitive to the bond thickness. Since the deformation in a cracked joint is highly localized at the crack tip, it is reasonable to use the Napkin Ring test results associated with very thin bonds (i.e., $h = 5 - 15$ μm). The latter is reproduced in Fig. 7 as a solid line, with the dotted line representing a smooth line fit. Because the FEM code requires the true stress vs.

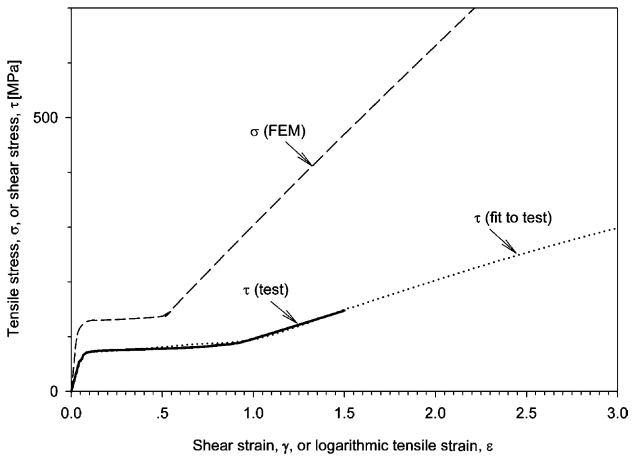

Fig. 7. Stress–strain relations for the adhesive used: heavy solid line—experimental shear stress vs. shear strain curve for a thin-bond adhesive (Chai, 1993b), dotted line—the behavior adopted, dashed line—the tensile stress vs. logarithmic tensile strain, which, when used in the FEA, reproduces the experimental response (i.e. the dotted line).

logarithmic strain response under uniaxial tension as input, it is necessary to convert shear to tensile response. Using a trial and error scheme on a model uniaxial configuration, the tensile stress vs. logarithmic tensile strain represented by the dashed curve is obtained. This result is used in the FEA.

A quasi-static analysis and a stationary crack are assumed. Plane-stress and plane-strain conditions are assumed for the adherends and the adhesive, respectively. This is except for a small strip of adhesive at the crack tip vicinity, where a distinct material model is used (Section 3.3.1). The post-yield behavior of the adhesive is modeled according to the J2 flow theory, i.e., with isotropic strain hardening and incremental plasticity theory based on the von Mises invariant. Large-strain, four-node isoparametric elements (Type 182) are used. As shown in Fig. 8, a fine mesh consisting of square elements of length Δ is constructed around the crack tip. Convergence of the solution is assessed by continuously refining the mesh. Up to 20,000 elements are found necessary to insure convergence of the local deformation field.

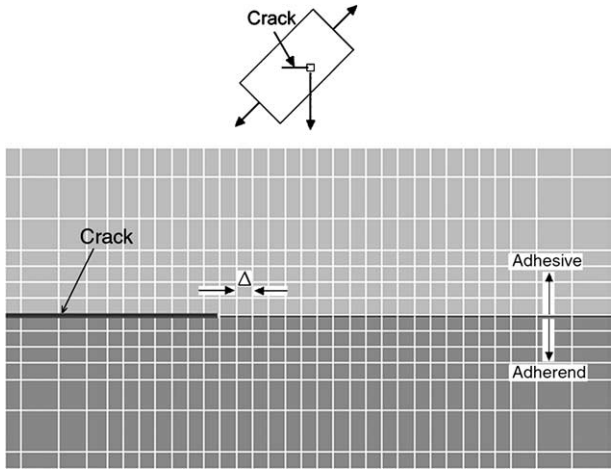

Fig. 8. FEM mesh at the vicinity of the tip of the interfacial crack.

The loading points of the scarf joint are pulled apart by a force P that is applied over a number of load steps. Both the loading points are free to rotate, in consistency with the tests. We define local parameters ε_{Av} and γ_{Av} as the bond-average tensile and shear strains at the crack tip (i.e., the relative normal and tangential displacements across the bond divided by the bond thickness). These quantities, which are easily determined from the distortion of the FEM grid, provide unambiguous (in the sense that they are insensitive to the mesh size or the material model of the fracture process zone) measure of local loading conditions, free of structural effects. In this way, the scarf angle θ is eliminated from the presentations in favor of the local loading phase angle ϕ.

3.2. Crack tip loading phase angle

Define a parameter f as

$$f = \tan\theta/\tan\phi \tag{4}$$

where ϕ is defined in Eq. (2). It can be easily shown from geometric considerations that $f = 1$ or $\phi = \theta$ in the special case of a homogeneous scarf joint subject to a uniform far field loading. For the present finite-size, pin-loaded joint, the adherends rotate during the loading. This introduces a relative displacement shift across the bond leading to a change in f. Fig. 9 shows FEA predictions for the variation of this quantity with the average shear strain in the bond, γ_{Av} (as calculated from the distortion of the FEM grid) for three different scarf angles. The data, specified to $h = 50$ μm, show that f is only mildly sensitive to the scarf angle while decreasing somewhat with increasing the load. The latter phenomenon is clearly dictated by the post-yield behavior of the adhesive. In the small-deformation regime, $f \approx 0.5$, which is 50% of the value obtained had the deformation and rotation of the adherends been neglected. The fact that f varies somewhat with γ_{Av} implies that the phase angle ϕ is not strictly fixed during crack propagation. This may be responsible to some of the observed variations in the experimental local shear strain during crack propagation. Nevertheless, the constancy of the local shear strain had ϕ been strictly fixed during crack propagation is clear from the data presented.

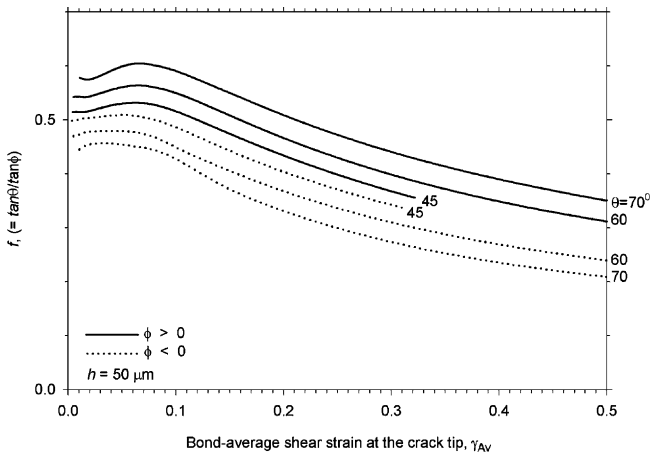

Fig. 9. FEM prediction for the variations of the bond-average strain ratio at the crack tip, f, with the bond-average shear strain at the crack tip. Results are given for various scarf angles, all corresponding to $h = 50$ μm. Curves are fits to discrete FEM data points. The solid and the dotted lines correspond to positive and negative phase angles, respectively.

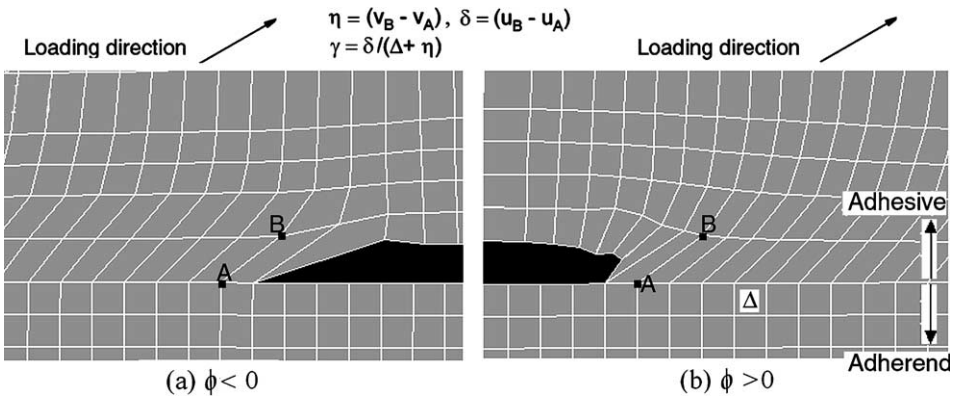

Fig. 10. The deformed FEM grid at the crack tip region for the case $h = 50$ μm, $\theta = 60°$ and $\gamma_{Av} = 0.1$: (a) negative phase angle, (b) positive phase angle. The local crack tip displacements are evaluated based on the relative normal and tangential displacements of the nodes marked A and B.

3.3. Local strain analysis

3.3.1. The model

To possibly eliminate the bond thickness dependence of the fracture (Fig. 6), the local deformation at the crack tip must be considered. Our approach is based on a fracture process zone possessing a distinct material response, and a scheme for extracting interface normal and tangential displacements within this zone. The experimental bond-average critical shear strain at the crack tip serves as a key feature in establishing critical values for the local displacements.

As can be seen from Figs. 2 and 3, the immediate crack tip vicinity undergoes extensive damage (i.e., voids and cavities), which must be accounted for in any quantitative local analysis. While this damage is difficult to model analytically, its net effect in this context is to cause stress relaxation at the crack tip vicinity through volume change. To bring out the essence of the present approach in the simplest way possible, we employ a rather straightforward though efficient scheme, namely retaining the plane-strain condition everywhere in the bond except for a small strip of adhesive near the crack tip vicinity, termed "fracture process zone", where a plane-stress condition is assumed. In effect, this implies that the material in the fracture process zone is composed of individual, unconnected strands of material. The lateral contraction of these strands leads to the desired volume change following the yielding of the adhesive. [4] The problem is further simplified by restricting the extent of the fracture zone to include only the first two rows of elements above the interface. A systematic study was carried out to elucidate the effect of the longitudinal dimension of this zone on the local displacements. The results for the most severe deformation used in this study show that the nodal displacements at the crack tip tend to reach steady-state values once the lengths of the process zone ahead and behind the crack tip are increased from approximately 10% and 2%, respectively, of the bond thickness. These values are thus used in the followings.

To calculate crack tip displacements, a fine grid consisting of square elements of equal size, Δ, is implemented at the immediate crack tip vicinity (Fig. 8). Fig. 10 illustrates the distorted grid near the crack tip

[4] It is well known that the yielding behavior of polymeric materials is pressure-sensitive. Madhusudhana and Narasimhan (2002) used the pressure-sensitive extended Drucker–Prager model in their cohesive zone analysis of mixed-mode fracture of adhesively bonded joints. Owing to the apparent lack of an appropriate flow rule for polymers subject to a combined loading and undergoing very large deformation and damage, the implementation of such a model at this stage of our analysis is probably premature.

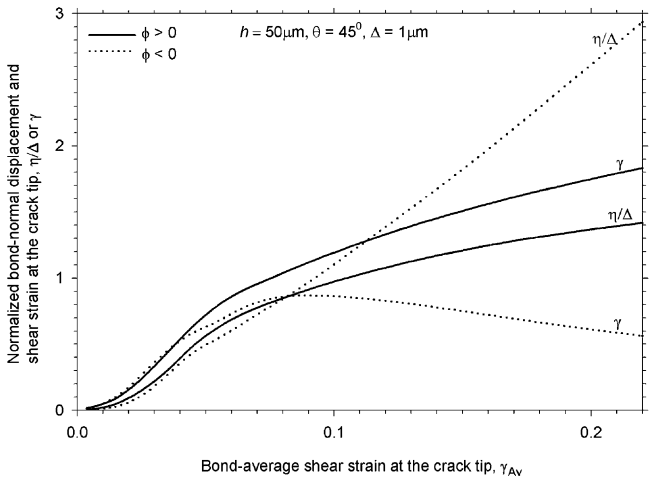

Fig. 11. FEM predicted crack tip local displacement parameters as a function of bond-average shear strain for the case $h = 50$ μm, $\theta = 45°$ and $\Delta = 1$ μm. The solid and the dotted lines correspond to positive and negative phase angles, respectively. The *critical local* displacement parameters are obtained when γ_{Av} becomes equal to its experimental counterpart (as given in Table 1).

for a choice of problem parameters. Let v and u denote the nodal displacements normal to the interface and along the interface, respectively. We define local crack tip displacements η and δ, respectively, as the bond-normal and tangential relative displacements between the two near-tip grid points marked A and B in Fig. 10:

$$\eta = v_B - v_A, \quad \delta = u_B - u_A \tag{5a}$$

Now define a local shear strain γ as

$$\gamma = \delta/(\Delta + \eta) \tag{5b}$$

Note that γ is consistent with the experimentally measured local shear strain at the crack tip (i.e., the local slope of a scratch line). Fig. 11 shows the variations of the ratio η/Δ and γ with the load applied to the scarf joint, represented by the FEM calculated γ_{Av}, for a given scarf angle (45°) and bond thickness (50 μm). In this presentation, $\Delta = 1$ μm. One observes that the sign of the phase angle significantly alters the behavior of the local deformation parameters once global yielding of the bond takes place. In this range, the trends for η/Δ and γ begin to depart. Data such as these are used next to predict critical local displacements.

3.3.2. Crack propagation analysis

FEA are performed for all the bond configurations detailed in Table 1, and the results in each case are presented as in Fig. 11. Fracture is taken to occur once γ_{Av} becomes equal to its experimental counterpart, given in Table 1. This facilitates a pair of FEM critical local parameters η/Δ and γ for a given specimen configuration (i.e., scarf angle and bond thickness). Fig. 12 summarizes the results for the choice $\Delta = 1$ μm, where the filled and the open symbols correspond to positive and negative phase angles, respectively. [5] For a given scarf angle, the normalized local parameters in Fig. 12 are virtually independent of the bond thickness. The combined results seem to conform reasonably well to a common linear relation

[5] Excluded from this presentation are some configurations pertaining to large scarf angles, where interpenetration of the materials across the crack face occurs. A proper treatment of this phenomenon requires a contact analysis, which is beyond the scope of this work.

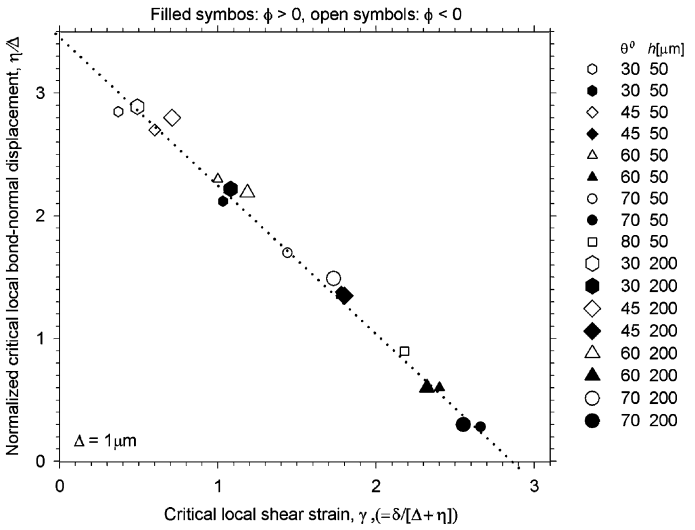

Fig. 12. FEM predicted relationship between the critical local shear strain and the normalized critical bond-normal displacement. Results are shown for various scarf angles and two bond thickness, i.e., 50 μm (small symbols) and 200 μm (large symbols); $\Delta = 1$ μm. Filled and open symbols denote positive and negative phase angles, respectively. The dotted line is a linear fit.

(dotted line). The ability of the present approach to combine the crack systems associated with the positive and the negative phase angles into a single universal relation is to be noted. It is now apparent that the difference in the experimental values of the critical local shear strains between these two cases for a given scarf angle (i.e., Fig. 5a and b) is a consequence of the different *local* mode-mixity conditions. It should be noted that attempts to present the fracture data in Fig. 12 in terms of the critical local displacements η vs. δ (instead of η/Δ vs. γ), in the spirit of the Tvergaard and Hutchinson model (1994), did not appear to produce a meaningful, single-valued relationship. (This, in fact, can be easily verified using the data of Fig. 12.)

Consider next the effect of the grid size Δ on the critical local crack tip parameters. For this purpose, data similar to those shown in Fig. 12 were generated for other values of Δ, i.e., 0.5 and 1.5 μm, all for $h = 50$ μm. The results, after appropriate normalization, are shown in Fig. 13. It can be seen that the entire data of this figure are reasonably well described by Eq. (6) below

$$\eta/\eta_c + \gamma/\gamma_c = 1, \quad \eta_c = 3.3 \ \mu\text{m}, \quad \gamma_c = 3, \tag{6}$$

where η_c and γ_c are the extreme bond-normal displacement and tangential strain, respectively. It is interesting to note that both of these quantities seem little sensitive to the mesh size, Δ. The insensitivity of η_c to Δ indicates that the bond-normal displacement at the crack tip is highly localized. One observes that the value of γ_c ($\approx$3) differs from its experimental counterpart (i.e., 1.33). It is found that if γ from the FEM is scaled by the factor 2.3 ($= 3/1.33$), than its variation with ϕ is quite similar to that of its experimental counterpart given in Fig. 6. Then, from Eq. (6), one would obtain a true value for η_c as 1.4 μm. Eq. (6) seems to constitute a viable fracture criterion due to its independence on the bond thickness or the sign of the phase angle. Furthermore, in light of the constancy of the local shear strain during crack propagation that was observed in the tests (rate effects excluded), one expects this criterion to hold true as well for a quasi-statically propagating crack. The effect of rate on crack propagation can be incorporated into Eq. (6) by making use of Eq. (1). The result is

$$\eta/\eta_c + \gamma/\gamma_c = 1 - \alpha(1 - e^{-\beta v}) \tag{7}$$

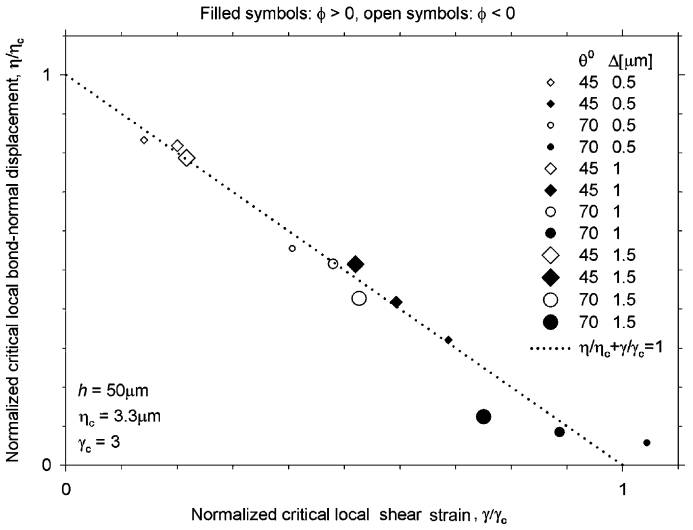

Fig. 13. FEM predicted relationship between the critical local shear strain and the critical bond-normal displacement. Results are given for three different FEM grid sizes, i.e., 0.5 μm (small symbols), 1 μm (intermediate size symbols) and 1.5 μm (large symbols), all specified to $h = 50$ μm. Filled and open symbols denote positive and negative phase angles, respectively. The dotted line curve is a linear fit. Note that the data are normalized by the extreme quantities η_c and γ_c.

Chai and Chiang (1998) have implemented a similar criterion in a finite-element scheme for studying crack propagation in adhesive bonds subject to pure mode II loading.

It is interesting to discuss how the present model may relate to other local fracture approaches. Xia and Shih (1995) have used a cohesive zone model in which a strip of voided cells is embedded in the bulk surrounding, straight ahead of the crack tip. The Gurson constitutive relation for dilatant plasticity (Gurson, 1977) was then used to describe hole growth in a cell. The latter leads to material softening and ultimate failure. Tvergaard (2001) employed a fracture process zone that is effectively represented by finite-thickness interface elements in the crack plane ahead of the crack tip. A porous ductile material model was used in the interface elements to represent the growth of voids to coalescence. The displacements of the interface elements are made compatible with the surrounding material. Such analyses entail local length scales such as the hole radius or the thickness of the element in the process zone. The present model may be viewed as conceptually similar, with the distinct plane-stress strip above the interface in this work playing the role of the cohesive or fracture process zone, and the thickness of the cohesive strip constituting the length scale. A noticeable difference with such studies is our use of local shear strain instead of the generally employed tangential displacement. This choice, however, is motivated by the fact that the shear strain is a physical quantity that may be directly measured in suitable tests. The viability of the local shear strain for predicting large-deformation fracture in homogeneous materials under simple shearing has been demonstrated by McClintock (1958), who proposed that crack propagation occurs when the shear strain a certain distance ahead of the crack tip reaches a critical value.

The present model can be applied to a new adhesive system similarly to common procedures for cohesive zone models (e.g., Kolhe et al., 1999; Madhusudhana and Narasimhan, 2002). The fact that only two parameters, i.e., η_c and γ_c, need be evaluated is advantageous. First, fracture tests are performed under pure mode I and mode II conditions, and the load needed to propagate a crack of given length is established. Then FEM simulation is performed, from which the two local parameters η_c and γ_c are extracted. By virtue of the independence of the fracture criterion on h, only a single bond thickness needs to be considered.

4. Discussions

It is interesting to examine how the local crack tip parameters may relate to the fracture energy. Detailed studies of mode II fracture in adhesive bonds (Chai, 1988), laminated composites (Hashemi et al., 1990) and mixed-mode fracture of adhesive bonds (Madhusudhana and Narasimhan, 2002) show that following a sub-critical growth during which the fracture energy monotonically increases, a steady-state value is reached. Figs. 2 and 4 vividly demonstrate that such resistance behavior may be attributed to the lateral spread of the intense deformation zone at the crack tip, with the steady-state phase taking over once that deformation becomes uniform across the bond. (As noted in Section 2.2, for relatively thick bonds or relatively large scarf angles, catastrophic growth may occur prior to the attainment of a uniform state deformation). The steady-state fracture energies under pure mode I and mode II conditions were determined experimentally for the present adhesive by Chai (1988). It was found that while $G_{\mathrm{IC}}^{\mathrm{ss}}$ is little sensitive to the bond thickness, $G_{\mathrm{IIC}}^{\mathrm{ss}}$ greatly increases with h, tending to a plateau when the latter is increased from about 150 μm. In the limit $h \to 0$, both $G_{\mathrm{IC}}^{\mathrm{ss}}$ and $G_{\mathrm{IIC}}^{\mathrm{ss}}$ converged to a common value, G_0 which was deemed an intrinsic property of the material. As proposed in Chai (1993b), the mode II steady-state fracture energy for relatively thin bonds (i.e., $h < 70$ μm) is well approximated by

$$G_{\mathrm{IIC}}^{\mathrm{ss}} = G_0 + \tau_{\mathrm{Y}} h \gamma_{\mathrm{Av}}^{\mathrm{ss}} \tag{8}$$

where $\gamma_{\mathrm{Av}}^{\mathrm{ss}}$ denotes the bond-average shear strain during steady-state growth while τ_{Y} is the yield stress in shear of the adhesive. Noting the coincidence of the "average" and the "local" shear strains during steady-state growth (e.g., Fig. 4a), one may substitute in Eq. (8) the critical *local* shear strain under pure mode II conditions, γ, for $\gamma_{\mathrm{Av}}^{\mathrm{ss}}$. In an attempt to extend this reasoning to mixed-mode loading, let the steady-state fracture energy in this case be written as

$$G_{\mathrm{C}}^{\mathrm{ss}} = G_0 + \tau_{\mathrm{Y}} h \gamma \tag{9}$$

As discussed above, this expression is consistent with the limit cases of pure mode I and mode II fracture. Using Eq. (3) to express γ in terms of the phase angle, ϕ, one has (for $h < 70$ μm)

$$G_{\mathrm{C}}^{\mathrm{ss}} = G_0 + Ah\tau_{\mathrm{Y}}(\mathrm{e}^{B\phi} - 1), \quad \phi > 0 \tag{10a}$$

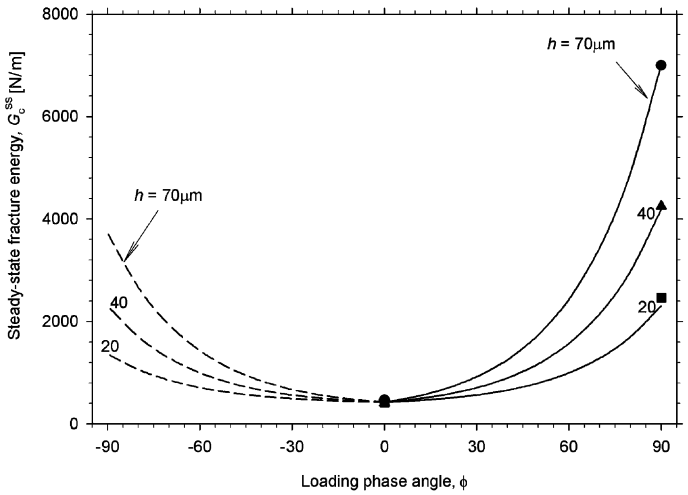

Fig. 14. The variations of the steady-state fracture energy of a joint with the loading phase angle for three different bond thickness. Curves are analytic predictions, symbols are experimental data for pure mode I and pure mode II loadings (Chai, 1988).

$$G_C^{ss} = G_0 + (A/2)h\tau_Y(e^{-B\phi} - 1), \quad \phi < 0, \tag{10b}$$

where A and B are given in Eq. (3). Fig. 14 (solid and dashed lines) shows the variations of G_c^{ss} with ϕ from Eq. (10) for three choices of bond thickness, i.e., 20, 40 and 70 μm. In this plot, G_0 and τ_Y are taken as 420 N/m and 70 MPa, respectively (Chai, 1988). Also shown as symbols are corresponding experimental results pertaining to the pure mode I and mode II cases (Chai, 1988). As shown, the agreement with the model is quite satisfactory. The fracture energy exhibits a pronounced asymmetry with respect to the sign of the phase angle. Recalling our discussion of the tendency of a crack associated with a negative phase angle to shift to the opposing interface prior to the attainment of steady-state crack propagation (see also Chai and Chiang, 1996), the fracture energy associated $\phi > 0$ should be considered. Finally, we note that the strong increase in the fracture energy with increasing the phase angle seen in Fig. 14 has been reported in a large number of investigations pertaining to bi-materials or adhesive bonding test specimens (e.g., Chai, 1988, 1992; Ferlund and Spelt, 1994; Brandenburger and Pearson, 1995; Tvergaard and Hutchinson, 1996; Swander and Liechti, 1998; Ducept et al., 2000; Madhusudhana and Narasimhan, 2002).

5. Summary and conclusions

A combined experimental/numerical effort is carried out using the scarf joint and the ENF specimens to elucidate the local fracture behavior of structural adhesive bonds subject to mixed-mode loading and undergoing large-scale yielding. Novel techniques for introducing a sharp interfacial pre-crack in the bond and for specimen surface decoration facilitate accurate determination of the bond-average and the local shear strains at the crack tip during the initial phase of crack propagation as well as the rest of the fracture event. The fracture, generally confined to an interface but always fully cohesive, is characterized by a slow growth phase that is followed by rapid or steady-state propagation. For a given mode mixity, the local shear strain is independent of the bond thickness, and, under quasi-static growth conditions, remains constant throughout the crack propagation event. This quantity is dependent on the crack speed and the magnitude and sign of the phase angle, however.

A large-strain finite-element analysis is used to obtain the deformation field at the tip of a stationary interfacial crack. To account for damage accumulation at the crack tip region during crack propagation, a simple material model allowing for volume change in the post-yield regime is used over a narrow strip at the crack tip region. The mode mixity of the joint is characterized by a local loading phase angle that is based on the ratio of the bond-average shear and tensile strains at the crack tip. A local fracture criterion is developed based on the tangential and normal displacements at the crack tip. Critical values for these parameters are determined with the aid of the load needed to cause crack propagation. The results from the various scarf angles employed in the tests seem to conform well to a universal local mixed-mode fracture criterion that seem independent of the bond thickness or the crack extension, and furthermore encompasses both the cases of positive and negative phase angles. The proposed approach thus isolates the effect of global structural response and global plastic deformation from the actual fracture process. This is in contrast to the fracture energy of the joint, which generally vary with the bond thickness and the crack extension. The local fracture criterion is governed by two parameters, η_c and γ_c, that seem little sensitive to the FEM grid. These quantities may be determined from relatively simple fracture tests.

The proposed approach is conceptually similar to cohesive zone models developed for bi-material interface crack problems. An apparent advantage of the present concept, particularly when large-scale yielding is involved, is that no traction-separation law need be invoked for the material at the fracture process zone. On the other hand, the need to specify the lateral extent of the damage zone in the present model is disadvantageous. This drawback may be circumvented, however, if a more sophisticated, continues type material model that incorporates volumetric changes in its flow rule is used. Treatment of the

pressure sensitivity of the yield behavior of the adhesive is another logical extension to this work. The experimentally obtained relationship between the critical bond-average shear strain and the local phase angle given in Fig. 6 or Table 1 may serve as useful input into such analyses.

References

Barret, J.D., Foschi, R.O., 1977. Engineering Fracture Mechanics 9, 371–378.

Bascom, W.D., Oroshnik, J., 1978. Effect of bond angle on mixed-mode adhesive fracture. Journal of Materials Science 13, 1411–1418.

Brandenburger, P.D., Pearson, R.A., 1995. Mixed mode fracture of organic chip attachment adhesives. In: Application of Fracture Mechanics in Electronic Packaging and Materials, ASME EEP-Vol. 11/MD-Vol. 64, pp. 179–184.

Chai, H., 1988. Shear fracture. International Journal of Fracture 37, 137–159.

Chai, H., 1990. Interlaminar shear fracture of laminated composites. International Journal of Fracture 43, 117–131.

Chai, H., 1992. Experimental evaluation of mixed-mode fracture in adhesive bonds. Experimental Mechanics 32, 296–303.

Chai, H., 1993a. Observation of deformation and damage at the tip of cracks in adhesive bonds loaded in shear and assessment of a criterion for fracture. International Journal of Fracture 60, 311–326.

Chai, H., 1993b. Deformation and failure of adhesive bonds under shear loading. Journal of Materials Science 28, 4944–4956.

Chai, H., Chiang, M.Y.M., 1996. A crack propagation criterion based on local shear strain in adhesive bonds subjected to shear. Journal of the Mechanics and Physics of Solids 44, 1669–1689.

Chai, H., Chiang, M.Y.M., 1998. A large strain analysis of Interfacial shear cracks in a constrained Interlayer; Part II—fracture. International Journal of Solids and Structures 35, 815–829.

Chowdhury, S.R., Narasimhan, R., 2000. A finite element analysis of stationary crack tip fields in a pressure sensitive constrained ductile layer. International Journal of Solids and Structures 37, 3079–3100.

Deepankar, D.E., Narasimhan, R., 1998. Analysis of interface fracture specimen for adhesively bonded joints. International Journal of Fracture 92, L35–L40.

Ducept, F., Davies, P., Gamby, D., 2000. Mixed mode failure criteria for a glass/epoxy composite and an adhesively bonded composite/composite joint. International Journal of Adhesion and Adhesives 20, 233–244.

Ferlund, G., Spelt, J.K., 1994. Mixed-mode fracture characterization of adhesive joints. Composite Science and Technology 50, 441–449.

Gurson, A.L., 1977. Continuum theory for ductile rupture by void nucleation and growth: Part I—yield criteria and flaw rules for porous ductile media. Journal of Engineering Materials and Technology 99, 2–15.

Hashemi, S., Kinloch, A.J., Williams, J.G., 1990. The effects of geometry, rate and temperature on mode I, mode II and mixed-mode I/II interlaminar fracture of carbon–fibre/Poly(ether–ether ketone) composites. Journal of Composite Materials 24, 918–956.

Ikeda, T., Yamashta, A., Lee, D., Miyazaki, N., 2000. Failure of ductile adhesive layer constrained by hard adherends. Journal of Engineering Materials and Technology 122, 80–85.

Kolhe, R., Tang, S., Hui, C.Y., Zehander, A.T., 1999. Cohesive properties of Nickel-alumina interfaces determined via simulation of ductile bridging experiments. International Journal of Solids and Structures 36, 5573–5595.

Liechti, K.M., Knauss, W.G., 1982. Crack propagation at materials interfaces: II experiments on mode interaction. Experimental Mechanics, 383–391.

Madhusudhana, K.S., Narasimhan, R., 2002. Experimental and numerical investigations of crack growth resistance of a ductile adhesive joint. Engineering Fracture Mechanics 69, 865–883.

McClintock, F.A., 1958. Ductile instability in shear. Journal of Applied Mechanics, 582–588.

Needleman, A., 1987. A continuum model for void nucleation by inclusion debonding. Journal of Applied Mechanics 54, 525–531.

Pang, H.L.J., Seetoh, C.W., 1997. A compact mixed mode (CMM) fracture specimen for adhesive bonded joints. Engineering Fracture Mechanics 57, 57–65.

Russell, A.J., Street, K.N., 1987. The effect of matrix toughness on delamination: static and fatigue fracture under mode II shear loading of graphite fiber composites. In: Toughened Composites, ASTM STP-937, pp. 275–294.

Suo, Z., Hutchinson, J.W., 1989. Sandwich test specimens for measuring interface crack toughness. Materials Science and Engineering A 107, 135–143.

Swander, J.G., Liechti, K.M., 1998. Asymmetric shielding mechanisms in the mixed-mode fracture of glass/epoxy interface. Journal of applied Mechanics 65, 25–29.

Trantina, G.G., 1972. Combined crack extension in adhesive joints. Journal of Composite Materials 6, 371–385.

Tvergaard, V., 2001. Crack growth predictions by cohesive zone model for ductile fracture. Journal of the Mechanics and Physics of Solids 49, 2191–2207.

Tvergaard, V., Hutchinson, J.W., 1993. The influence of plasticity on mixed mode interface toughness. Journal of the Mechanics and Physics of Solids 41, 1119–1135.

Tvergaard, V., Hutchinson, J.W., 1994. Toughness of an interface along a thin ductile layer joining elastic solids. Philosophical Magazine A 70 (4), 641–656.

Tvergaard, V., Hutchinson, J.W., 1996. On the toughness of ductile adhesive joints. Journal of the Mechanics and Physics of Solids 44, 789–800.

Xia, L., Shih, C.F., 1995. Ductile crack growth—I. A numerical study using computational cells with microstructurally-based length scales. Journal of the Mechanics and Physics of Solids 43, 233–259.

Yang, Q.D., Thouless, M.D., 2001. Mixed-mode fracture analysis of plastically deforming adhesive joints. International Journal of Fracture 110, 175–187.